Structure and Morphology of Polyethylene/Polypropylene In-Reactor Alloys Synthesized by Spherical High-Yield Ziegler–Natta Catalyst

Zhisheng Fu, Yanzhong Zhang, Zhiqiang Fan, Junting Xu

Department of Polymer Science and Engineering, The Institute of Polymer Science, Zhejiang University, Hangzhou 310027, People's Republic of China

Received 1 May 2005; accepted 20 September 2005
DOI 10.1002/app.23265
Published online in Wiley InterScience (www.interscience.wiley.com).

ABSTRACT: A series of spherical polyethylene/polypropylene (PE/PP) in-reactor alloys were synthesized with spherical high-yield Ziegler–Natta catalyst by sequential multistage polymerization in slurry. The morphology of PE/PP alloy granule was evaluated by optical microscopy, scanning electron microscopy, and transmission electron microscopy. The results show PE/PP in-reactor alloy with excellent morphology, high porosity, and narrow distribution of the particle size. The PE/PP in-reactor alloys show excellent mechanical properties with good balance between toughness and rigidity. It was fractionated into five fractions by temperature-gradient extraction fractionation, and every fractionation was analyzed by FTIR, ^{13}C-NMR, DSC, and WAXD. The PE/PP in-reactor alloy was found to contain mainly five portions: PP, PE, segmented copolymer with PP and PE segment of different length, ethylene-*b*-propylene copolymer, and an ethylene–propylene random copolymer. The characteristic chain structure leads to good compatibility between the fractions of the alloy that shows a multiphase structure. © 2006 Wiley Periodicals, Inc. J Appl Polym Sci 103: 2075–2085, 2007

Key words: polyethylene; polypropylene; alloys; structure; morphology

INTRODUCTION

Improving the impact strength of polypropylene (PP) to prepare toughened PP has been widely studied both in science and in industry.[1–6] Among the different ways to toughen PP, in-reactor blending of PP with other polyolefin (e.g., ethylene-propylene random copolymer) by sequential multistage polymerization has been proved superior with respect to both polymer properties and production cost.[7–9] Because of the high efficiency spherical Ziegler–Natta catalyst, the production of PP in-reactor alloy has been progressing since the 1990s.[10–12] Polypropylene/poly(ethylene-*co*-propylene) (PP/EPR) in-reactor alloy has been industrialized in large scale. However, as compared to PP homopolymer, this kind of toughened PP suffers from a significant drop in flexural modulus, since there is more than 10% of random copolymer (EPR) with low modulus in the alloy. A possible way of overcoming this drawback is to add polyethylene (PE) into the alloy, as PE is a crystalline polymer with moderate rigidity. Zhang et al.[13] prepared HDPE/PP blends by injection molding processes. It was found that HDPE/PP blends of high tensile strength (97.1 MPa) and high toughness (45.5 kJ/m^2) were obtained when the PP content in the blends was 8 and 20 wt % respectively, which were 4.3 and 9.5 times as high as the corresponding values of the pure PP, respectively. In our previous work,[7,9] we prepared polypropylene/polyethylene (PP/PE) in-reactor alloys using spherical Ziegler–Natta catalyst by multistage polymerization (first by homopolymerization of propylene and then by homopolymerization of ethylene). The PP/PE in-reactor alloys showed good balance between toughness and rigidity, especially at low temperature. For example, impact strength and flexural modulus of the sample containing 62.8 wt % PP were 653 J/m and 757 MPa at 23°C, respectively. The impact strength at –30°C of the sample is as high as 347 J/m. However, most of the PP/PE in-reactor alloy granules were broken and there was too much fine powder in the product that caused reactor fouling.

In this study, we changed the sequence of the polymerization process and a new type of spherical PE/PP in-reactor alloy granules were prepared by fore-and–aft polymerization of ethylene and propylene in slurry. The PE/PP in-reactor alloy showed excellent mechanical properties.[14] As reported in many literatures, high impact PP blends, produced either by copolymerizing propylene with ethylene or by blending

Correspondence to: Z.-Q. Fan (fanzq@zju.edu.cn).
Contract grant sponsor: Special Funds for Major State Basic Research Projects; contract grant number: 2005CB623800.
Contract grant sponsor: National Natural Science Foundation of China; contract grant number: 20474053.

Journal of Applied Polymer Science, Vol. 103, 2075–2085 (2007)

PP with various elastomers, show biphase or multiphase structure. As is well known, the effectiveness of toughening plastics like PP by blending with rubber depends on the morphology of the blend, such as the shape of the dispersed phase, its size and distribution, the morphology of the matrix, and the degree and nature of adhesion between different phases.[8,15] Up to date, there are few literatures reporting synthesis of PE/PP in-reactor alloys by multistage polymerization, and their chain structure, morphology, and properties. In this article, we will study the morphology of the PE/PP in-reactor alloys and try to correlate it with the structure and properties of the polymer. Since PE is a crystalline polymer with moderate rigidity, as the multistage polymerization proceeding PP disperses into the PE matrix, unique features in morphology and structure of the PE/PP in-reactor may be expected.

EXPERIMENTAL

Preparation of PE/PP in-reactor alloy

A high-yield spherical $TiCl_4/MgCl_2$·ID (ID, internal donor) catalyst (DQ-1, kindly donated by the Beijing Research Institute of Chemical Industry) was used in the polymerization reaction, with $Al(C_2H_5)_3$-$Ph_2Si(OCH_3)_2$ as a cocatalyst in slurry in petroleum ether. The PE/PP in-reactor alloys were synthesized by a three-stage slurry polymerization process. The first stage was propylene prepolymerization in petroleum ether for about 3 min at 40°C under 0.1 MPa propylene. The next stage was successive ethylene polymerization at 53°C under 0.6 MPa ethylene in an autoclave. And the last stage is propylene polymerization at 53°C under 0.5 MPa propylene for a predetermined period of time. The monomer of the previous stage was removed by an evacuation when switching the polymerization from one stage to another. In the first stage, prepolymer of PP with spherical morphology was produced. In the second stage, spherical PE granules of 1.0–2.0 mm diameter with high porosity were produced. After the third stage, in-reactor PE/PP alloy granules of 1.0–2.0 mm diameter and relatively low porosity were obtained. Ethylene content in PE/PP in-reactor alloys could be controlled by changing the duration of ethylene or propylene polymerization or by varying the other polymerization conditions.

Morphology of PE/PP in-reactor alloy

The internal morphology of the cross section of PE/PP in-reactor alloy granules was recorded by an optical camera.

The films of PE/PP in-reactor alloys for transmission electron microscope (JSM-T20) observation were prepared by casting a 0.5 wt % solution of the polymer in xylene on the surface of glycol at 120°C.

The intersection morphology of PE/PP in-reactor alloy particle was observed using JSM-T20 scanning electron microscope.

Fractionation of PE/PP in-reactor alloy

The PE/PP in-reactor alloys were fractionated according to crystallinity by temperature-gradient extraction fraction (TGEF). The room temperature (20°C) fraction was separated by dissolving 5 g of sample in boiling *n*-octane, and the soluble part was recovered by concentrating the solution and precipitation in ethanol. The insoluble part was used for the next fractionation steps. A modified Kumagawa extractor (made by us) was used to carry out TGEF of the insoluble part. *n*-Octane was used as the solvent to successively extract the polymer at different controlled temperatures. Three fractions were collected at 100, 113, and 120°C, respectively. The 120°C insoluble part was taken as the last fraction. Therefore, five fractions, with extraction temperature of 20, 100, 113, 120, and >120°C, were collected from a PE/PP alloy sample. Purified fractions were obtained by concentrating the extract solution, precipitating the polymer, and washing and drying the fractions in vacuum.

FTIR analysis of PE/PP in-reactor alloys and fractions

FTIR spectra of PE/PP in-reactor alloys and the fractions were recorded on a Bruker Vector 22 FTIR spectrometer. Thin film of the sample was prepared by hot-pressing. The ethylene content of the polymer sample was calculated according to the equation

$$C_2(\text{mol \%}) = 37.2990 + 57.817lg\frac{A_{720}}{A_{1166}} + 27.287\left(\lg\frac{A_{720}}{A_{1166}}\right)^2$$

which was obtained by measuring the FTIR of PE/PP blends of known composition.[14]

^{13}C-NMR analysis of the fractions

^{13}C-NMR spectra of the fractions were measured on a Bruker AMX400 NMR spectrometer at 100 MHz. *o*-Dichlorobenzene-d4 was used as solvent to prepare the polymer solution of 20 wt %. The spectra were recorded at 120°C, with hexamethyldisiloxane as internal reference. Broadband decoupling and a pulse delay of 5 s were employed. Typically 3000 transients were collected.

DSC analysis of the fractions

Differential scanning calorimetry (DSC) analysis of the fractions were made on a PerkinElmer Pyris 1 DSC instrument under N_2 atmosphere. About 5 mg of sample was sealed in aluminum sample pan, and the fractions were first annealed at 140, 130,120, 110, 100, 90, 80, 70, and 60°C, respectively, each for 12 h. Then the DSC scan was recorded at a heating rate of 5°C/min.

WAXD analysis of fractions

Samples for wide angle X-ray diffraction (WAXD) analysis in the form of $30 \times 20 \times 1$ mm^3 plate were prepared by first melt-pressing the alloy at 230°C for 2 min and then annealing at 130°C for 3 h. A Rigagu DmaxrA X-ray diffractometer was used to record the WAXD graphs, and the crystallinity of the samples was calculated from the areas of the diffraction peaks (representing the crystalline phase) and the halo (representing the amorphous phase).

PLM analysis

Samples for polarized light microscope observation were prepared by fusing small piece of the polymer placed between two cover glasses. After melting at 230°C for 2 min, they were kept at 130°C for 30 h. Photographs were taken using a LEICA DM LM polarized microscope.

Measurement of the particle porosity

The measurement of the particle porosity was carried out in a density bottle of weight W_0. The volume of the weighted density bottle (V) was calibrated by *n*-butanol. The density bottle filled with polymer particle was weighed (W_1) and then filled with *n*-butanol. The density bottle was put into a thermostatic bath for 4 h, dried, and then weighed (W_t). The following equation was used to calculate the bulk density of polymer granules (ρ_b):

$$V = \frac{W_{\text{polymer}}}{\rho_b} + \frac{W_t - W_1}{\rho_{\text{n-butanol}}}$$

where W_{polymer} is the weight of polymer granules, $\rho_{n\text{-butanol}}$ is the density of *n*-butanol.

The apparent density of polymer granules ρ_{app} can be measured by substituting mercury for *n*-butanol. The porosity of polymer granules (P) can be calculated using the following equation:

$$P = 1 - \frac{\rho_{\text{app}}}{\rho_b}$$

Measurement of the mechanical and physical properties

The notched Charpy impact strength of the alloy samples was measured on a Ceast impact strength tester according to ASTMD 256. The flexural modulus and flexural strength were measured following ASTMD 709 on a REGER-2000 electronic tester. The alloy granules were heat-molded at 170°C into sheets, which were then cut into pieces, put into a $150 \times 150 \times 4$ mm^3 mold, and pressed under 25 MPa at 180°C for 5 min. The sample plates were then slowly cooled to room temperature in the mold. Sample strips for the tests were cut from the plate, following ASTM. For each test point, five parallel measurements were made and the average values were adopted.

RESULTS AND DISCUSSION

Morphology and mechanical properties of PE/PP in-reactor alloys

Excellent morphology of polyolefin particles is very important for industrial processing. The internal morphology of cross section of PE granules, PE/PP in-reactor alloy granules, and PP/PE in-reactor alloy granules are shown in Figure 1. As shown in Figure 1, it is hard to find difference between PE granules and PE/PP in-reactor granules from the external morphology, which are spherical or oval. However, it is obvious that the external morphology of PE/PP in-reactor alloy granules is much better than that of PP/PE in-reactor alloy granules. In addition, it was found that more than 80 wt % of PE/PP in-reactor alloy granules fall in the diameter range of 1.0–1.5 mm by sieving samples.

To reveal the internal morphology of PE/PP in-reactor alloy granules, the SEM of intersection surface of PE/PP in-reactor alloy granules was examined. Figure 2 is the internal morphology of PE granule and PE/PP in-reactor alloy granule. PE granule has bigger pore and higher porosity, which is due to serious diffusion limitation in the ethylene polymerization. At the same reaction conditions, the solubility of ethylene is lower than that of propylene in petroleum ether, and the polymerization activity of ethylene is much higher than that of propylene. So the mass transfer limitation would lead to the formation of concentration gradient inside the growing polymer granules, with the concentration decreasing from outside to inside. Ethylene primarily polymerizes at the external surface of the growing polymer. It is difficult for ethylene to diffuse into the core of the growing polymer granules, and so there is big a pore formed in PE granules. However, the solubility of propylene in petroleum ether is higher than that of ethylene under the same conditions, but the polymerization activity of propylene is relatively low. Hence propylene can eas-

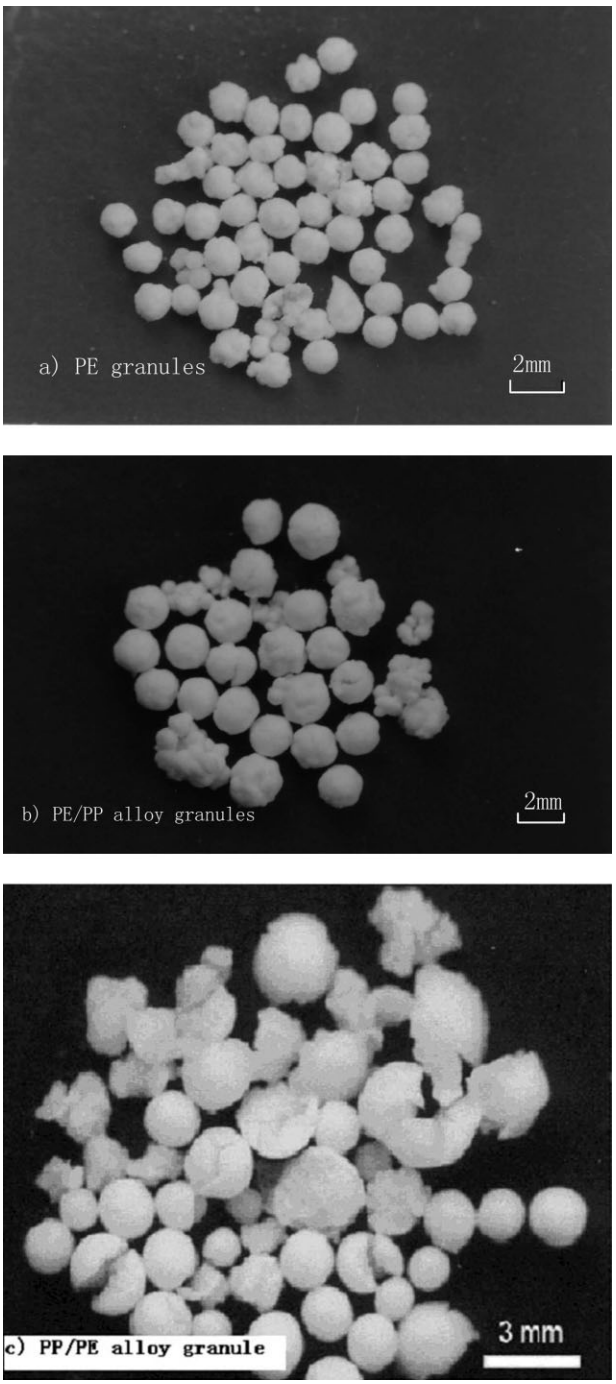

Figure 1 External morphology of PE, PE/PP alloy, and PP/PE alloy granules.

ily diffuse into the center of the growing particle. With the increase in time of propylene polymerization, the pore size and the porosity of polymer granules decreased and the propylene content of PE/PP in-reactor alloys increased. As shown in Figure 3, with the increase in the content of PP in the products, the bands at 998 and 841 cm^{-1}, which represent isotactic PP chains, becomes stronger. Meanwhile, the doublet bands at 720–730 cm^{-1} caused by the crystallization of PE segments gradually decreased. In Table I, as the content of PP in the alloys increases, from sample EP-1 to sample EP-5, the porosity of PE/PP in-reactor alloys decreases. Sample EP-5 has the highest content of propylene in the alloy and the lowest porosity.

The data in Table I show that the impact strength of the PE/PP in-reactor alloy (56.5–130 kJ/m^2) is much higher than that of homopolypropylene (7.7 kJ/m^2). Obviously, it is efficient to toughen PP by the three-stage polymerization process designed in this study. At the same time, the PE/PP in-reactor alloys possess high flexural modulus (1370–2450 MPa). It means that the PE/PP in-reactor alloys show excellent mechanical properties with good balance between toughness and rigidity. As the content of ethylene in PE/PP in-reactor alloys increases, the impact strength of the alloy increases gradually, whereas the flexural modulus decreases.

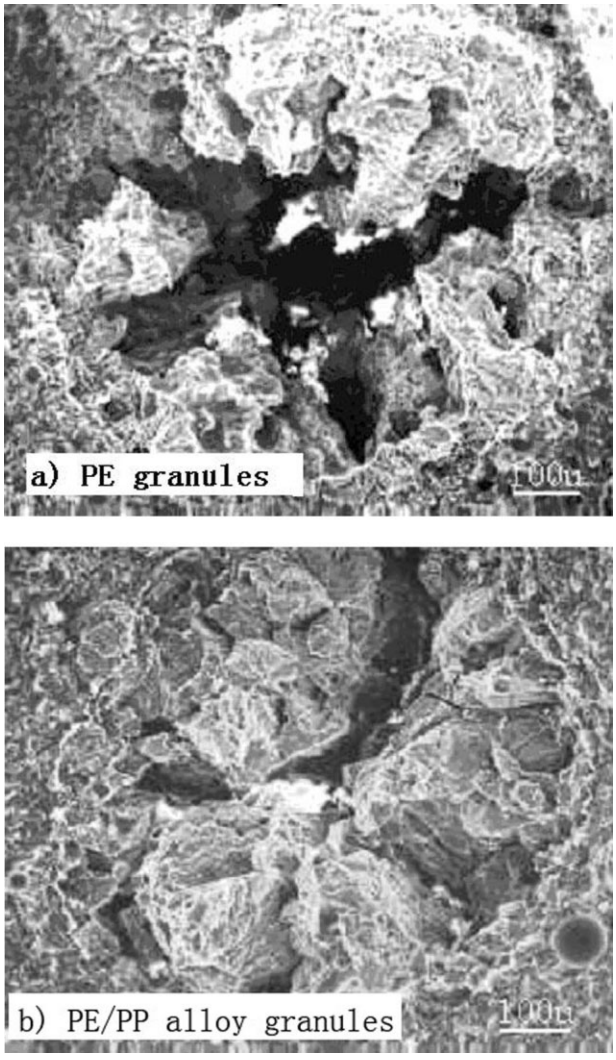

Figure 2 SEM of cross section of PE and PE/PP in-reactor alloy granules.

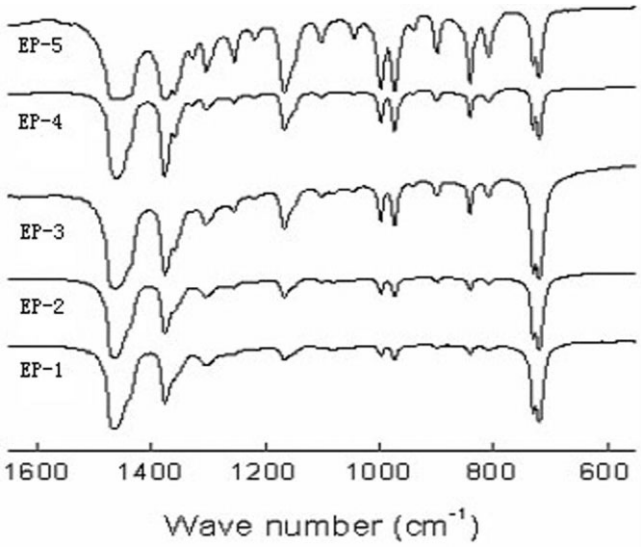

Figure 3 FTIR spectra of PE/PP in-reactor alloys.

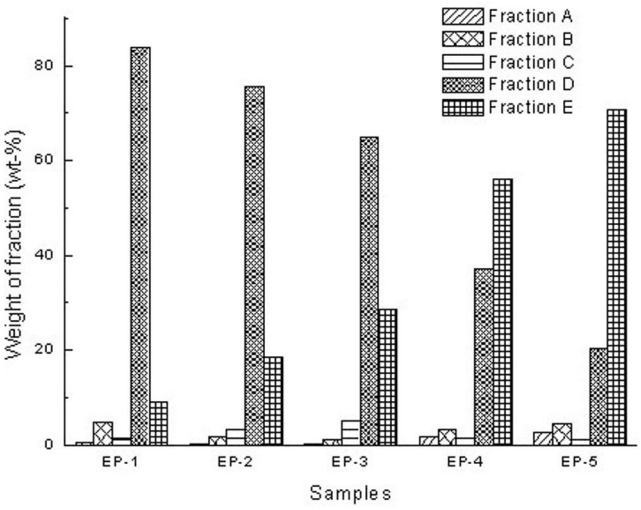

Figure 4 Fraction distributions of the PE/PP in-reactor alloys.

Chain structure of the PE/PP in-reactor alloy

The PE/PP in-reactor alloys were fractionated by TGEF into five fractions, and the results are shown in Figure 4. The parts soluble at room temperature, 100, 113, and 120°C are named as fraction A, B, C, and D, respectively. And the insoluble residue at 120°C is fraction E. It can be seen that fraction D and fraction E constitute the main portion of the in-reactor alloys, which account for more than 90 wt %. From sample EP-1 to sample EP-5, the content of fraction D decreases gradually, whereas the content of fraction E increases gradually.

As shown in Figure 5, all the five fractions of sample EP-5 were analyzed by FTIR. In the fraction A and fraction B, the doublet bands at 720–730 cm^{-1}, which are caused by the crystallization of PE segments, are very weak. This means that the PE segments are too short to crystallize. The doublet bands of the fraction C are visible at 720–730 cm^{-1}, indicating that part of the PE segments are long enough to form crystalline lamellae. In the other two fractions, the doublet bands at 720–730 cm^{-1} are clearly seen. Meanwhile, the bands at 998 and 841 cm^{-1} are also detectable in these two fractions. This means that both ethylene and propylene segments in fractions C, D, and E are crystallizable.

Based on the relative intensity of the characteristic IR bands of PE and PP, the change of ethylene content in the fractions with extraction temperature can be rationalized, and is shown in Table II. It is found that the relative intensity of PE bands increases gradually in the former four fractions, showing that the ethylene content increases with extraction temperature. However, the intensity of PE bands in the last fraction is relatively weak, meaning that there are few ethylene units in this fraction.

From the FTIR spectra of the five fractions, we can primarily conclude that fraction A is a random copolymer in which both PE segments and PP segments are too short to crystallize. The spectra of fraction B and fraction C are similar to that of fraction A, but the length of PE segment and PP segment increases gradually. The spectrum of fraction D shows that it is

TABLE I
Characteristics of PE/PP In-Reactor Alloy Granules

Sample	Polymerization time (min)		Catalyst efficiency (kg polymer/g Ti)	Content of polypropylene (mol %)	Porosity (vol %)	Notched Charpy impact strength (kJ/m^2)	Flexural strength (MPa)	Flexural modulus (MPa)
	Ethylene	Propylene						
EP-1	120	60	57.3	7.0	43	Not broken	25.4	720
EP-2	120	120	64.8	14.8	34	130	32.7	1370
EP-3	120	180	72.5	23.0	33	121	38.3	1490
EP-4	60	120	62.2	44.1	31	102	40.4	1670
EP-5	30	120	56.5	53.9	26	56.5	48.2	2450

Reaction conditions: Al/Ti = 120 (mol/mol); Si/Ti = 2.5 (mol/mol); reaction temperature = 53°C; ethylene pressure = 0.6 MPa; propylene pressure = 0.5 MPa.

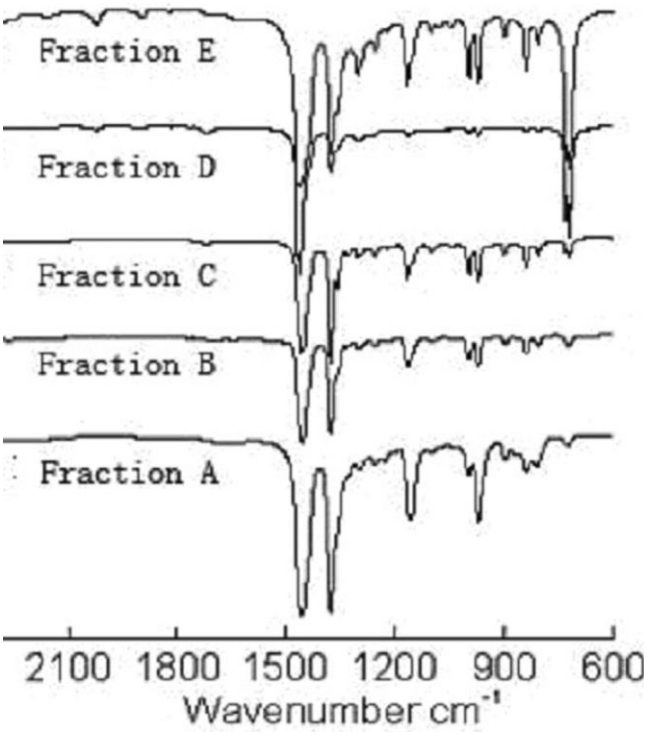

Figure 5 The FTIR spectra of the five fractions of PE/PP in-reactor alloy (sample EP-5).

composed of large amount of PE segments and trace amount of PP segment. The fraction E is composed of large amount of PP and small amount of PE.

To further explore the chain structure of the different fractions, ^{13}C-NMR spectra of fraction D and fraction E were recorded and are shown in Figure 6. The spectrum of the fraction D looks like the mixed spectra of large amount of PE with small amount of PP. It was calculated that the content of PE in the fraction D was 99 mol % based on the ^{13}C-NMR spectrum, which was very close to the results of FTIR analysis. The peaks at 35.7–36.0 ppm ($S_{\alpha\delta}$, $S_{\alpha\gamma}$), 31.3 ppm ($T_{\delta\delta}$), 25.4 ppm ($S_{\beta\delta}$), 22.9 ppm ($S_{\beta\beta}$), and 18.1 ppm ($P_{\delta\delta}$) are also visible in the spectra, indicating that there are also sequences such as PPEP, PPEE, EPE, and PEP in the chain.[16] In our previous work,[17] we found that PE

TABLE II
The Fraction Distribution of Sample EP-5 and Ethylene Content in Each Fraction

Fraction	Extraction temperature (°C)	Fraction content (wt %)	C_2 (mol %)
A	20	2.7	42.6
B	100	4.6	44.6
C	113	1.2	67.5
D	120	20.4	99.2
E	>120	70.8	22.3

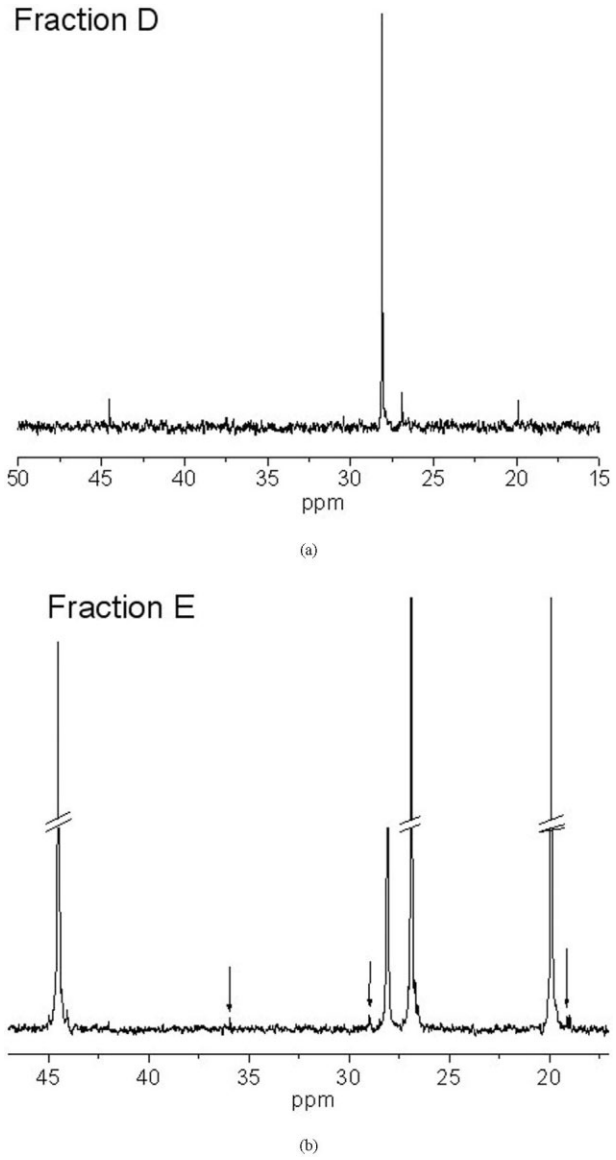

Figure 6 ^{13}C-NMR spectra of fraction D and fraction E of sample EP-5.

homopolymer fractions can be eluted at temperatures lower than 120°C in temperature rising elution fraction (TREF), and PP chains of high isotacticity are extracted by TGEF only at temperatures higher than 120°C. The possibility that these fractions are PE/PP mixture can be ruled out. Therefore, the PP segments are chemically linked with the PE segments and there exist ethylene–propylene block copolymer in the 120°C fraction. However, the presence of PE homopolymer cannot be excluded. Considering the nonliving characteristic of coordination polymerization and the wide extraction temperature range, we believe that the 120°C fractions are mixture of PE and PE-*b*-PP copolymer with very long PE segments and relatively short PP segments. The fraction E shows ^{13}C-NMR signals typical of PE (20 mol %) and PP (80 mol %). In

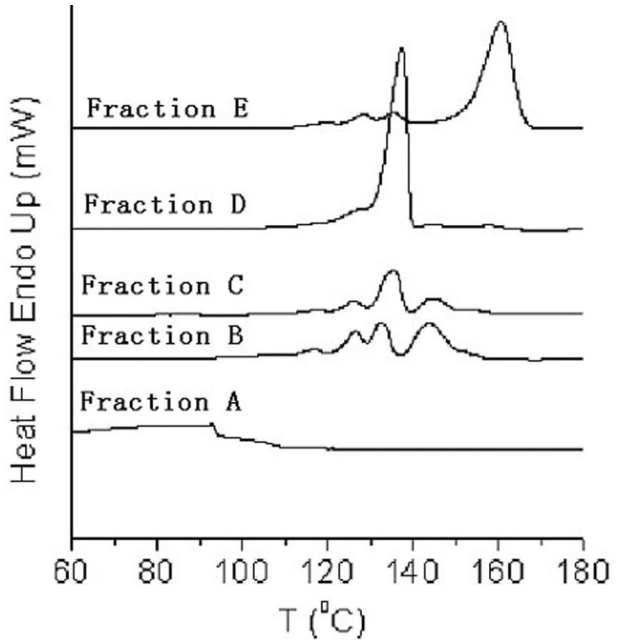

Figure 7 DSC thermogram of the five fractions of PE/PP in-reactor alloy (sample EP-5).

the spectrum, trace amount of conjunction structure between the PE segments and PP segments represented by the $S_{\alpha\delta}$, $S_{\beta\delta}$, or $T_{\beta\delta}$ peaks were detected, which is an evidence that the PE and PP segments are actually connected to form a block copolymer. Since there is a propylene homopolymerization stage in this three-stage process and PP chains of high isotacticity are extracted only by TGEF at temperatures higher than 120°C, we could conclude that the fraction extracted at $>$ 120°C are mixture of pure iPP and PE-*b*-PP block copolymer.

Thermal analysis of annealed samples was also conducted to verify the chain structures of different fractions. Multi-step annealing of the samples ensures that the PE and PP segments of different lengths form lamellae of different thickness, thus the DSC melting curve can reflect the presence of these different lamellae. The DSC heating scanning curves and WAXD graphs of the fractions are shown in Figures 7 and 8, respectively. As shown in Figure 7, DSC melting curves of the five fractions are very different from each other. Absence of endothermic peak in the range of 60–160°C on the DSC melting curves of fraction A means that it is completely amorphous. The fraction B and fraction C show several weak endothermic peaks in the range of 80–150°C, which are mainly formed by PE segments of different length. The WAXD graph of fraction B shows weak peaks at $2\theta = 21$ and 23, which are diffractions of the PE crystal planes (110) and.(200) There are also weak peaks at 17 and 14, which correspond to the (110) and (040) planes of PP crystal, which may also show their peaks in the range of 80–150°C in the DSC graph and make the curve more complicated. Therefore, in this fraction there are very small amount of PE and PP segments that can form imperfect crystals. As the extraction temperature rises to 113°C (fraction C), the WAXD peaks from PE become stronger, while the PP crystallinity is slightly decreased. In this fraction the main component should be an ethylene–propylene copolymer that contains many long PE segments, and the length of PE segments is distributed in a rather broad range. The melting curve of the fraction D shows two melting peaks at temperatures similar to that of PE (137°C) and PP (160°C), respectively. However, the peak at 160°C is very weak. From the ^{13}C-NMR results, we know that the fraction D is a mixture of PE/PE-*b*-PP. Thermal analysis also shows that PE homopolymer accounts for the major part of this fraction. In the fraction D, the PE diffraction becomes the strongest, which is consistent with its high ethylene content. Finally, in the fraction E ,both the peaks from iPP crystalline and PE crystalline are observed in the WAXD graph. The PP diffraction becomes very strong, whereas the PE diffraction becomes relatively weak. The DSC melting curve of fraction E shows a strong peak at 161°C and two weak peaks in the range of 120–140°C, meaning that it is mainly composed of pure PP besides a little PE-*b*-PP block copolymer with very long PP segments and short PE segments.

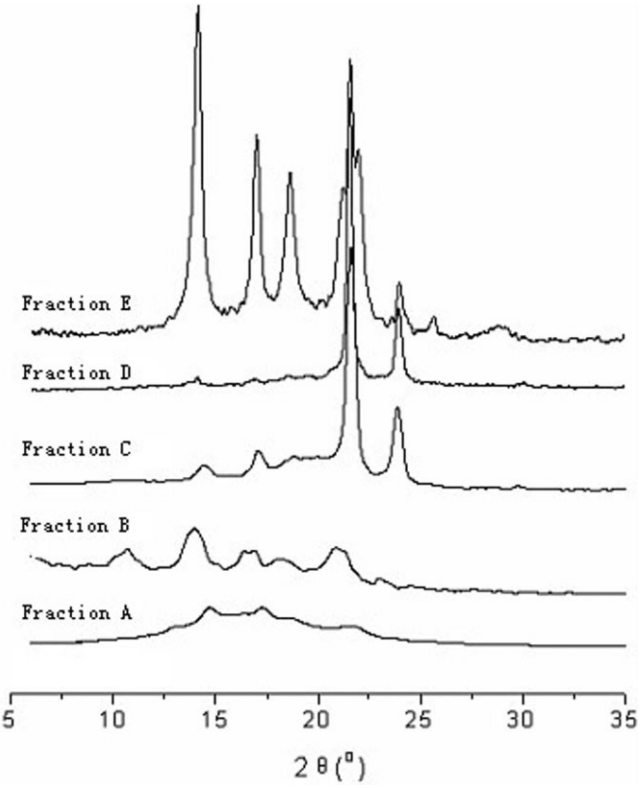

Figure 8 WAXD graphs of the five fractions of PE/PP in-reactor alloy (sample EP-5).

By combining the results of IR, NMR, DSC, and WAXD analysis, we can get a clear map of the chain structure and structure distribution of the PE/PP in-reactor alloy. PE homopolymer is mainly found in the 120°C fraction, and PP homopolymer exists in the >120°C fraction. These two fractions constitute more than 90 wt % of the alloy. The 113°C fraction is mainly composed of block copolymer with many long PE segments, and the length of PE segments is distributed in a rather broad range. This fraction constitutes 1.2–5.2 wt % of the alloy. Other two components, ethylene–propylene random copolymer (EPR) and ethylene–propylene segmented copolymer, are also present in the PE/PP in-reactor alloys. To understand this phenomenon, we should consider the PE-*b*-PP block copolymer formed at the very beginning of the homopolymerization of propylene after the ethylene homopolymerization. At the beginning of the propylene homopolymerization, many of the active centers still have chemically bonded PE propagation chains that are formed in the ethylene homopolymerization stage. When these active centers meet propylene monomer in the second stage, copolymerization happens on these living PE chains, forming block copolymers with long PE segments. After a chain-transfer reaction, such block copolymer chains will leave the active centers, and the chains formed later will be mainly random copolymer chains. Obviously, PE and PP form in the homopolymerization stage of ethylene and propylene respectively. The PE and PP components have distinct mechanic properties, and the presence of segmented copolymer and PE-*b*-PP block copolymer ensures high interfacial adhesion among different phases. Such unique chain structure of the PE/PP in-reactor alloys leads to the excellent balance between stiffness and toughness.

Crystalline structure

Optical microscopy can give more evidence, which may help to decide the chain structure of the fractions. The crystalline morphology of the four fractions of sample EP-5 was observed by PLM and is shown in Figure 9. As a contrast, Figure 9(E,F) show the crystalline morphology of pure PP and pure PE, respectively. Figure 9(E) shows typical PP spherulites, with variations from the Maltese cross-pattern imposed by their mixed birefringence. Figure 9(F) shows typical PE spherulites, with Maltese cross-pattern and concentric rings. The PLM image of fraction E (insoluble part at 120°C; Figure 9(A)), is comparatively similar to the PLM image of pure PP, but the spherulites are much smaller than that of pure PP. Formation of more irregular spherulites in fraction E indicates that there is not only PP but also other components that confine the crystallization of PP in fraction E. This is consistent to the result of thermal analysis. The PLM image of fraction D [Figure 9(B)], is comparatively similar to the PLM image of pure PE with subtle concentric rings. But the spherulites are smaller than that of pure PE. Figure 9(C,D) are PLM images of fraction C and fraction B, respectively. In these two images almost no spherulites can be observed; however, the amorphous phase appears obviously. These results further verify the chain structure of the fractions as revealed by the FTIR, NMR, DSC, and WAXD analysis.

The crystalline morphology of the isothermal crystallized in-reactor alloys was also studied by PLM. The PLM image of pure PE [Fig. 9(F)] shows typical banded spherulites, with variations from the Maltese cross-pattern imposed by their mixed birefringence. As shown in Figure 10, at propylene content of only 7.0 mol %, irregular spherulite of PE were formed, but when the propylene content was increased to 23.0 or 53.9 mol %, almost no perfect spherulites could be observed. The crystalline phase was quite irregular and randomly scattered. The average size of the crystalline domains became smaller as propylene content increased. This shows that the PE matrix is partly compatible with the PP phase with the aid of the segmented copolymer portion in the alloy. This caused significant phase mixing between the PE phase and the PP phase and then reduces the size of the crystalline domains.

Transmission electron microscopy (TEM) examination of cast films substantiated phase separation in PE/PP in-reactor alloy. TEM micrographs of PE/PP in-reactor alloy samples with different PE content are showed in Figure 11. Figure 11(A) is a TEM micrograph showing the semicrystalline morphology of the pure PE homopolymer. A loosely developed spherulitic structure is observed in pure PE, with clustering of long PE crystalline lamella that appears ribbon-like. Clearly, the PE lamella is very long (on the order of a micrometer) compared to their thickness (on the order of 10 nm). Figure 11(B) shows a TEM micrograph of the PE/PP in-reactor alloy containing 23.0 mol % PP. Lamella in the sample is more irregularly aligned and shorter than that in pure PE. Figure 11(C) shows a TEM micrograph of the PE/PP in-reactor alloy containing 53.9 mol % PP. There is almost no perfect crystalline lamella. The length of the lamella (50–100 nm) is the smallest in these three samples. Comparing Figure 11(A) with Figure 11(B,C), the crystalline lamella observed in those two PE/PP in-reactor alloys are much shorter (in dimension perpendicular to PE chain stem) than those observed in PE. This effect can be ascribed to confinement of the PE crystallization within the microphase-separated PE domains. The crystallization lamellae and crystallinity

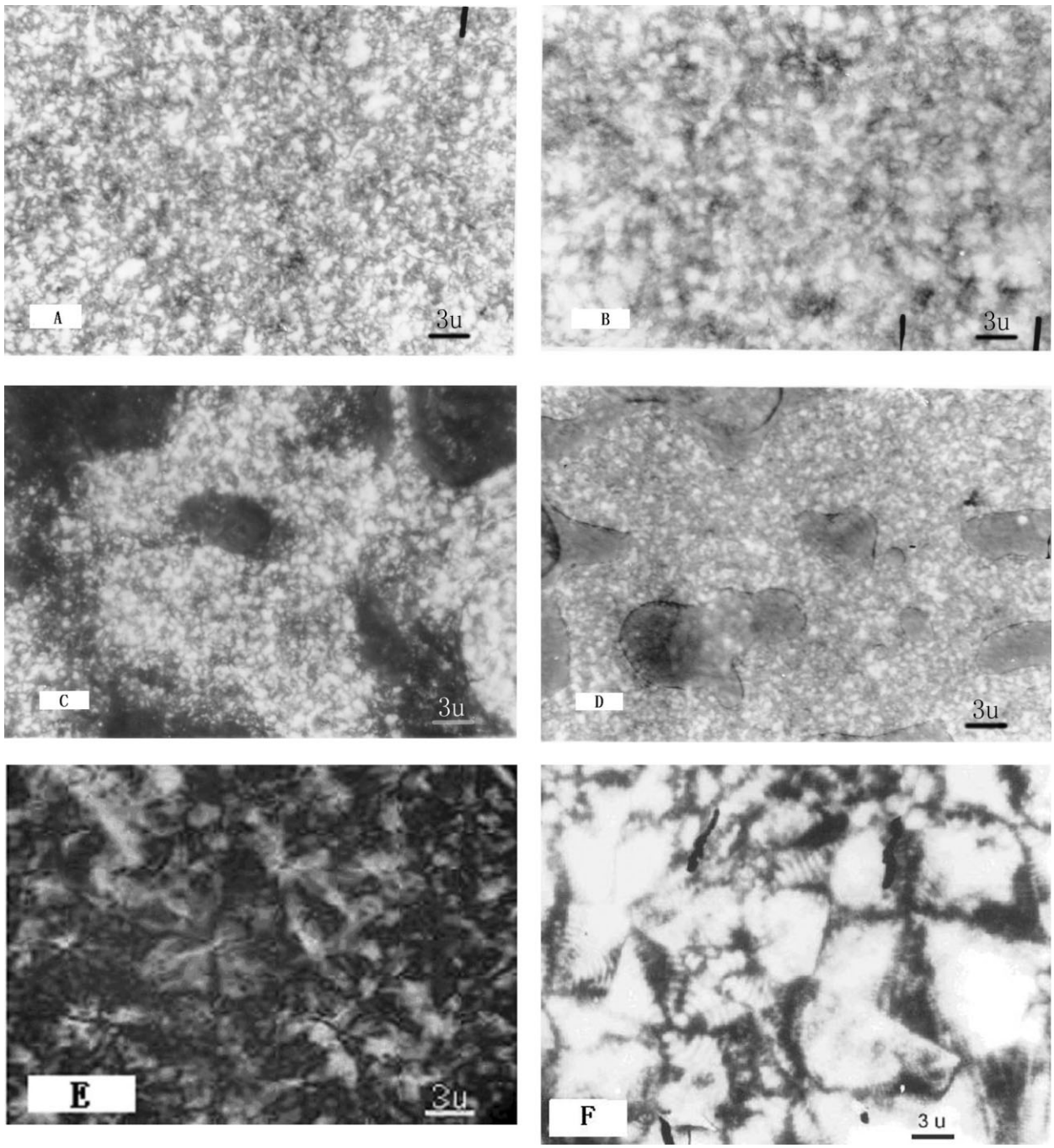

Figure 9 PLM photographs of different fractions of PE/PP in-reactor alloy (sample EP-3) crystallized isothermally at 120°C for 24 h. (A) 120°C insoluble fraction; (B) 120°C fraction; (C) 113°C fraction; (D) 100°C fraction; (E) pure PP; (F) pure PE.

of PE are affected by other component miscible or partly miscible with PE in the PE/PP in-reactor alloy. As the PP content increased to 53.9 mol % in the PE/PP in-reactor alloy, phase mixing between the PE and PP phases becomes significant. Such high degree of phase mixing could hinder the formation of regular spherulites and reduce the size of the crystalline domains.

CONCLUSIONS

By sequential multistage slurry polymerization, PE/PP in-reactor alloys with spherical morphology and good flowability can be produced. The PE/PP in-reactor alloys show excellent mechanical properties, with good balance between impact strength and flexural modulus. As the content of PP in PE/PP in-

reactor alloys increases, the impact strength of the PE/PP in-reactor alloys decreases gradually, whereas their flexural modulus increases. The alloy contains mainly five portions: random ethylene–propylene copolymer (EPR), segmented ethylene–propylene copolymer, ethylene-*b*-propylene copolymer, PE, and PP. The chain structure of the fractions of the PE/PP in-reactor alloy changes gradually from fraction A to fraction E, and so their morphology changes from noncrystalline to semicrystalline. The characteristic chain structure leads to good compatibility between the fractions of the alloy, which shows a multiphase structure. The PLM images and TEM micrographs show that as the content of propylene in the alloy increases, the degree of phase mixing increases.

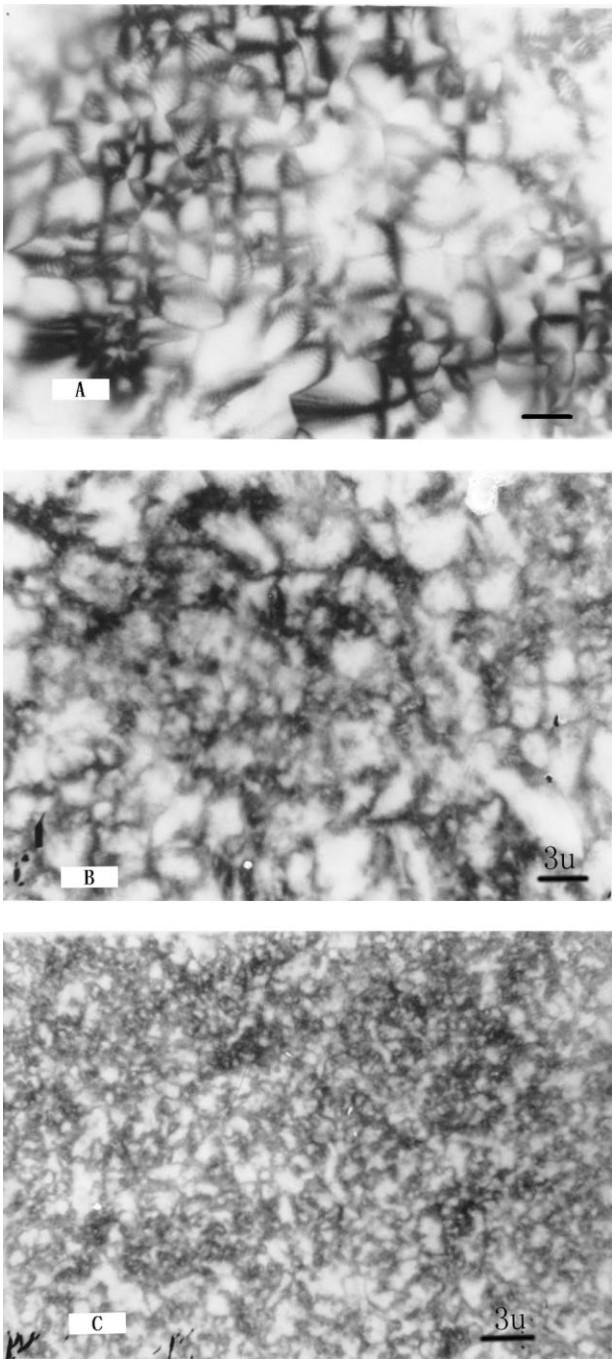

Figure 10 PLM photographs of pure PE and PE/PP in-reactor alloy ((A) pure PE; (B) sample EP-1; (C) sample EP-3; (D) sample EP-5.

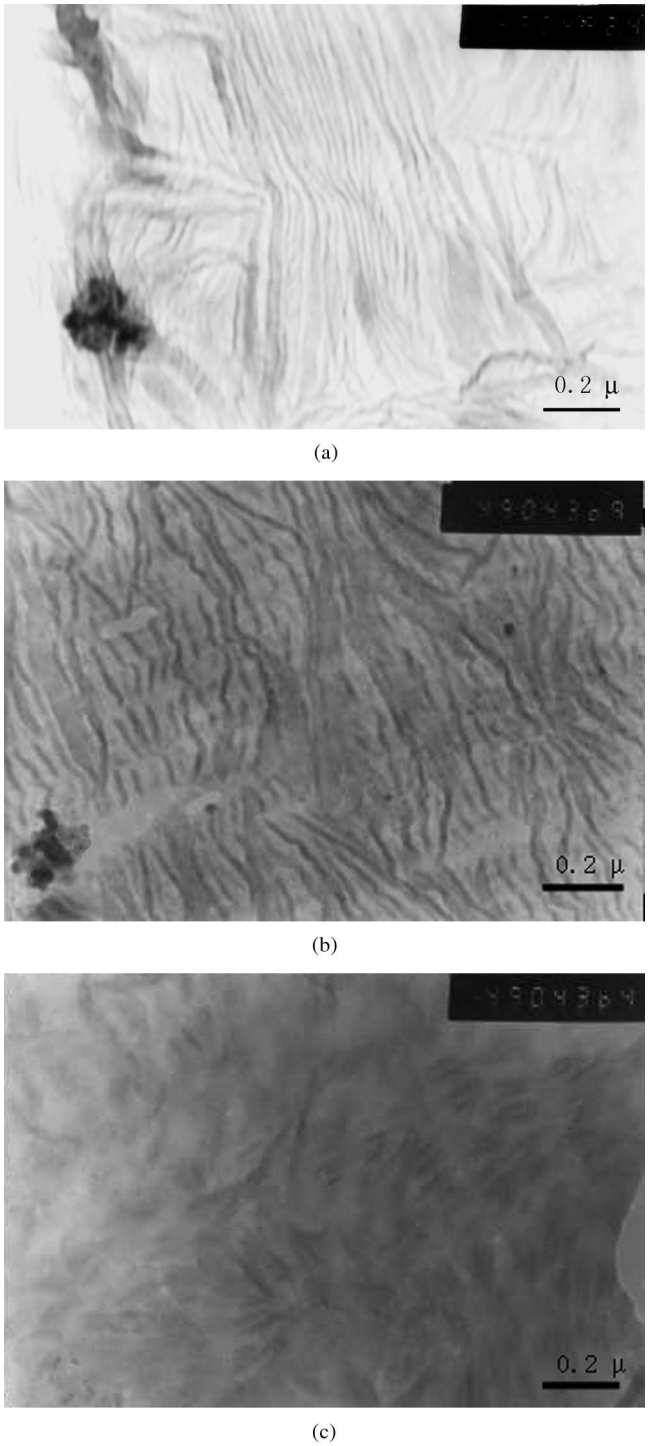

Figure 11 Transmission electron micrographs of cast films of PE and PE/PP in-reactor alloys.

References

1. Collina, G.; Pelliconi, A.; Sgarzi, P.; Sartori, F.; Baruzzi, G. Polym Bull 1997, 39, 241.
2. Van der Wal, A.; Mulder, J. J.; Oderkerk, J.; Gaymans, R. J Polym 1998, 39, 6781.
3. Liang, J. Z.; Li, R. K. Y. J Appl Polym Sci 2000, 77, 409.
4. Galli, P.; Vecellto, G. Prog Polym Sci 2001, 26, 1287.
5. Pukanszky, B.; Tudos, F.; Kallo, A. Polymer 1989, 30, 1399.
6. Xu, Z. K.; Zhu, Q. Q.; Feng, L. X.; Yang, S. L. Makromol Chem Rapid Commun 1990, 11, 79.
7. Zhang, Y. Q.; Fan, Z. Q.; Feng, L. X. J Appl Polym Sci 2002, 84, 445.
8. Liu, N. C.; Baker, W. E. Polymer 1994, 35, 988.
9. Fan, Z. Q.; Zhang, Y. Q.; Xu, J. T.; Wang, H. T.; Feng, L. X. Polymer 2001, 42, 5559.
10. Galli, P.; Hay, J. C. Makromol Chem Macromol Symp 1992, 63, 19.
11. Kittilsen, P.; McKenna, T. J Appl Polym Sci 2001, 82, 1047.
12. Galli, P. Prog Polym Sci 1994, 19, 959.
13. Zhang, G.; Fu, Q.; Shen, K. Z.; Jiang, L. Acta Polym Sin 2000, 3, 306.
14. Zhang, Y. Z. Ph.D. Thesis, Zhejiang University, Hangzhou, People's Republic of China, 2003.
15. Kukaleva, N.; Jollands, M.; Cser, F.; Kosior, E. J Appl Polym Sci 2000, 76, 1011.
16. Tritto, I.; Fan, Z. Q.; Locatelli, P.; Sacchi, M. C.; Camurati, I.; Galimberti, M. Macromolecules 1995, 28, 3342.
17. Xu, J. T.; Fu, Z. S.; Fan, Z. Q.; Feng, L. X. Eur Polym J 2002, 38, 1739.